A&A, 697, A7 (2025)
https://doi.org/10.1051/0004-6361/202450793


Astronomy & Astrophysics

*Euclid on Sky* Special issue

# *Euclid*: Early Release Observations – A glance at free-floating newborn planets in the $\sigma$ Orionis cluster*

E. L. Martín[1,2,**], M. Žerjal[1,2], H. Bouy[3,4], D. Martin-Gonzalez[5], S. Muñoz Torres[1,2], D. Barrado[6], J. Olivares[7], A. Pérez-Garrido[8], P. Mas-Buitrago[6], P. Cruz[6], E. Solano[6], M. R. Zapatero Osorio[6], N. Lodieu[1,2], V. J. S. Béjar[1,2], J.-Y. Zhang[1,2], C. del Burgo[1,2], N. Huélamo[6], R. Laureijs[9], A. Mora[10], T. Saifollahi[11,12], J.-C. Cuillandre[13], M. Schirmer[14], R. Tata[15], S. Points[16], N. Phan-Bao[17,18], B. Goldman[19,11], S. L. Casewell[20], C. Reylé[21], R. L. Smart[22,23], C. Dominguez-Tagle[1,2], A. Escobar[1], N. Sedighi[1,2], S. Tsilia[1,2], N. Vitas[1,2], A. Ayadi[3,4], N. Aghanim[24], B. Altieri[25], S. Andreon[26], N. Auricchio[27], M. Baldi[28,27,29], A. Balestra[30], S. Bardelli[27], A. Basset[31], R. Bender[32,33], D. Bonino[22], E. Branchini[34,35,26], M. Brescia[36,37,38], J. Brinchmann[39], S. Camera[40,41,22], V. Capobianco[22], C. Carbone[42], J. Carretero[43,44], S. Casas[45], M. Castellano[46], S. Cavuoti[37,38], A. Cimatti[47], G. Congedo[48], C. J. Conselice[49], L. Conversi[50,25], Y. Copin[51], L. Corcione[22], F. Courbin[52], H. M. Courtois[53], M. Cropper[54], A. Da Silva[55,56], H. Degaudenzi[57], A. M. Di Giorgio[58], J. Dinis[55,56], F. Dubath[57], X. Dupac[25], S. Dusini[59], A. Ealet[51], M. Farina[58], S. Farrens[13], S. Ferriol[51], P. Fosalba[60,61], M. Frailis[62], E. Franceschi[27], M. Fumana[42], S. Galeotta[62], B. Garilli[42], W. Gillard[63], B. Gillis[48], C. Giocoli[27,64], P. Gómez-Alvarez[65,25], A. Grazian[30], F. Grupp[32,33], L. Guzzo[66,26], S. V. H. Haugan[67], J. Hoar[25], H. Hoekstra[68], W. Holmes[69], I. Hook[70], F. Hormuth[71], A. Hornstrup[72,73], D. Hu[54], P. Hudelot[74], K. Jahnke[14], M. Jhabvala[75], E. Keihänen[76], S. Kermiche[63], A. Kiessling[69], M. Kilbinger[77], T. Kitching[54], R. Kohley[25], B. Kubik[51], M. Kümmel[33], M. Kunz[78], H. Kurki-Suonio[79,80], D. Le Mignant[81], S. Ligori[22], P. B. Lilje[67], V. Lindholm[79,80], I. Lloro[82], D. Maino[66,42,83], E. Maiorano[27], O. Mansutti[62], O. Marggraf[84], N. Martinet[81], F. Marulli[85,27,29], R. Massey[86], E. Medinaceli[27], S. Mei[87], M. Melchior[88], Y. Mellier[89,74], M. Meneghetti[27,29], G. Meylan[52], J. J. Mohr[33,32], M. Moresco[85,27], L. Moscardini[85,27,29], S.-M. Niemi[9], C. Padilla[90], S. Paltani[57], F. Pasian[62], K. Pedersen[91], W. J. Percival[92,93,94], V. Pettorino[9], S. Pires[13], G. Polenta[95], M. Poncet[31], L. A. Popa[96], L. Pozzetti[27], G. D. Racca[9], F. Raison[32], R. Rebolo[1,2], A. Renzi[97,59], J. Rhodes[69], G. Riccio[37], Hans-Walter Rix[14], E. Romelli[62], M. Roncarelli[27], E. Rossetti[28], R. Saglia[33,32], D. Sapone[98], B. Sartoris[33,62], M. Sauvage[13], R. Scaramella[46,99], P. Schneider[84], A. Secroun[63], G. Seidel[14], M. Seiffert[69], S. Serrano[60,100,101], C. Sirignano[97,59], G. Sirri[29], L. Stanco[59], P. Tallada-Crespí[43,44], A. N. Taylor[48], H. I. Teplitz[102], I. Tereno[55,103], R. Toledo-Moreo[104], A. Tsyganov[105], I. Tutusaus[106], L. Valenziano[27,107], T. Vassallo[33,62], G. Verdoes Kleijn[12], Y. Wang[102], J. Weller[33,32], O. R. Williams[105], E. Zucca[27], C. Baccigalupi[108,62,109,110], G. Willis[54], P. Simon[84], J. Martín-Fleitas[10], and D. Scott[111]

*(Affiliations can be found after the references)*

Received 20 May 2024 / Accepted 25 July 2024

**ABSTRACT**

We provide an early assessment of the imaging capabilities of the *Euclid* space mission to deeply probe nearby star-forming regions and associated very young open clusters, and in particular, to determine to which extent it can shed light into the newborn free-floating planet population. This paper focusses on a low-reddening region observed in just one *Euclid* pointing. The dust and gas has been cleared out from the region by the hot $\sigma$ Orionis star. One late-M and six known spectroscopically confirmed L-type ultracool members in the $\sigma$ Orionis cluster were used as benchmarks to provide a high-purity procedure to select new candidate members with *Euclid*. The exquisite angular resolution and depth delivered by the *Euclid* instruments allowed us to focus on bona fide point sources. A cleaned sample of $\sigma$ Orionis cluster substellar members was produced, and the initial mass function (IMF) was estimated by combining *Euclid* and *Gaia* data. Our $\sigma$ Orionis substellar IMF is consistent with a power-law distribution without a significant steepening at the planetary-mass end. No evidence of a low-mass cutoff is found down to the detection limit of this study at 4 Jupiter masses in the very young $\sigma$ Orionis open cluster.

**Key words.** catalogs – surveys – astrometry

## 1. Introduction

The nearest star-forming regions provide us with a natural laboratory to investigate the complex processes in detail that transform molecular clouds into stellar- and substellar-mass objects. In particular, one of the long-standing questions is whether there is a low-mass cutoff in the IMF, which was originally defined by Salpeter (1955) as a single power-law function over the mass range from 10 down to 0.4 solar masses ($M_\odot$). While the early computations of spherical collapse including

* This paper is published on behalf of the Euclid Consortium.
** Corresponding author; ege@iac.es

dust-grain opacities found a minimum mass of 0.1 $M_{\odot}$ owing to opacity-limited fragmentation, that is, above the substellar-mass limit (Silk 1977), recent calculations predict that the minimum fragment could reach down to $10^{-3}\,M_{\odot}$ (Mondal & Chattopadhyay 2019), which is well below the deuterium-burning mass limit. The thermonuclear fusion of deuterium, $^{2}$H(p,$\gamma$)$^{3}$He, takes place at $10^{6}$ K and can be strong in the early stages of evolution of objects with masses above 13 times the mass of Jupiter (1 $M_{\rm J}$ = 0.000955 $M_{\odot}$) (see Bodenheimer 1966, Stahler 1988, and Chabrier et al. 2000).

Deep observations of stellar nurseries, very young open clusters, and young stellar associations have been made to search for the predicted low-mass cutoff of the IMF, and it was reported that the IMF extends smoothly into the realm of planetary masses, reaches down to the deuterium limit and overlaps with the masses of exoplanets. Various names have been used to refer to these unexpected substellar-mass objects, such as brown dwarfs (BDs) of planetary mass, sub-brown dwarfs, cluster planets, nomadic worlds, free-floating planets (FFPs), rogue planets, and planetary-mass objects (PMOs). Collectively, substellar-mass objects are ultracool dwarfs (UCDs) with very cool effective temperatures, late spectral types, small sizes, and faint luminosities that cause them to appear to be a tiny minority among the myriad stars and galaxies in deep astronomical surveys, even though their numbers can be significant.

Free-floating planets appear to be ubiquitous and numerous because they have been identified by direct imaging and spectroscopy in many different stellar cradles. Some examples of these targets are the Chamaeleon I star-forming region (Oasa et al. 1999; Luhman et al. 2004); the IC 348 and NGC 1333 clusters in Perseus (Esplin & Luhman 2017; Scholz et al. 2023), the Ophiuchus star-forming region (Chiang & Chen 2015; Bouy et al. 2022), the Orion nebula cluster (Lucas & Roche 2000; Lucas et al. 2001, 2006), the Lynds 1630 molecular clouds (Spezzi et al. 2015), the $\sigma$ Orionis (Zapatero Osorio et al. 2000; Lodieu et al. 2009) and Collinder 69 (Bayo et al. 2011) young clusters in the Orion giant star formation complex, the Upper Sco OB association (Lodieu et al. 2018, 2021; Miret-Roig et al. 2022), and the Taurus dark clouds (Esplin & Luhman 2019). PMOs have also been found as wide companions to stars and BDs (Chauvin et al. 2005; Gauza et al. 2015), as members of young moving associations (Zhang et al. 2021), and as microlensing events towards the Galactic bulge (Mróz et al. 2018; Koshimoto et al. 2023; Sumi et al. 2023).

The existence of FFPs challenges models of star and planet formation. A variety of physical mechanisms have been proposed to explain the formation of substellar objects with masses well below the Jeans limit, the leading one being turbulent fragmentation (Padoan & Nordlund 2004; Hennebelle & Chabrier 2008), but others, including gravitational collapse in filaments, ejection from proto-planetary discs, and photo-erosion (Miret-Roig 2023), have not been discarded as potential players.

The cosmology-driven requirements of the *Euclid* mission (Laureijs et al. 2011) and the performance of its VISible instrument (VIS; Euclid Collaboration: Cropper et al. 2025) and Near-Infrared Spectrometer and Photometer (NISP; Euclid Collaboration: Jahnke et al. 2025) are expected to enable a major leap in sensitivity gain and area coverage that will foster the advance of many areas of legacy science in astrophysics (Euclid Collaboration: Mellier et al. 2025), including the detection of about one million UCDs over a large portion of the Milky Way (Solano et al. 2021; Martin et al. 2023), with spectroscopic reconnaissance spectra for thousands of them (Martín et al. 2021; Zhang et al. 2024). The *Euclid* reference observing sequence (ROS) is the main observation mode that is used for the wide and deep surveys. It is required to reach limiting AB magnitudes of 26.2 in the optical $I_{\rm E}$ band and of 24.5 in the near-infrared NISP bands over a wide area (Euclid Collaboration: Scaramella et al. 2022).

The *Euclid* Early Release Observations (ERO) programme has been designed to be a showcase of the potential for legacy science across a wide range of sky regions. It demonstrates that *Euclid* brings a unique combination of unprecedented sensitivity, wide-area coverage, and high spatial resolution to the investigation of diverse science topics. The first ERO papers include studies of very high redshift objects (Weaver et al. 2025), clusters of galaxies (Atek et al. 2025; Kluge et al. 2025; Marleau et al. 2025; Saifollahi et al. 2025), nearby galaxies (Hunt et al. 2025), and galactic globular clusters (Massari et al. 2025).

This ERO paper investigates the power of *Euclid* to probe deep into very young regions over a wide area, reaching detection limits capable of revealing the FFP population and searching for the predicted low-mass cutoff of the IMF. The paper is structured as follows. In Sect. 2, the general *Euclid* ERO project 2 (ERO02; P.I. Martín) is presented. Five *Euclid* pointings were obtained, and this work focuses on about half of the area that is covered by one of them. In Sect. 3, the particular region that is the focus of this work is described, and in Sect. 4 we discuss previously known substellar-mass objects in the $\sigma$ Orionis cluster and present the cuts we used to select new FFP candidates. Section 5 describes the revised IMF of the $\sigma$ Orionis cluster in the area covered by the *Euclid* observations and compares it with the field IMF low-mass tail. Finally, Sect. 6 summarises our results and provides future prospects.

## 2. The *Euclid* Early Release Observations project of nearby star-forming regions

This *Euclid* ERO programme has targeted nearby (distance ≤400 pc) star-forming regions and very young open clusters (age <10 Myr) to explore their faint ultracool populations, search for FFPs, and determine whether there is an IMF low-mass cutoff. The total project consists of five *Euclid* pointings. The targets were the NGC 1333 cluster in Perseus (incomplete dataset), Barnard 30, Barnard 33 (the Horsehead nebula, which also includes the NGC 2023 embedded cluster and part of the $\sigma$ Orionis open cluster), the Messier 78 dark clouds in the Orion star formation complex, and a field containing several dark clouds in the Taurus region. In this paper, we focus on one of these targets, called the Horsehead field, and in particular, we focus on about half of the area, hereafter called the ERO-SOri field. The other regions covered by the *Euclid* ERO pointings will be the subject of future studies.

The *Euclid* observation of the ERO-SOri field took place on 2 October 2023. A full ROS with good guiding was obtained. The centre coordinates of each of the four *Euclid* exposures that make up the ROS were 85°.150915, −2°.613342, 85°.167068, −2°.582078, 85°.166265, −2°.551255, and 85°.182417, −2°.519991. The full field of view (FoV) of the ERO pointing presented here is displayed in Fig. 1 and covers an area of 0.58 square degrees. The FoV was chosen to avoid the blinding star $\sigma$ Orionis and to include the Barnard 33 molecular cloud, the NGC 2023 cluster and reflection nebula, and the IC 434 H II region. The full *Euclid* ROS consisted of four dithered exposures in VIS and NISP using the nominal exposure times described in Euclid Collaboration: Cropper et al. (2025) and Euclid Collaboration: Jahnke et al. (2025), respectively. The dithering pattern was designed so that

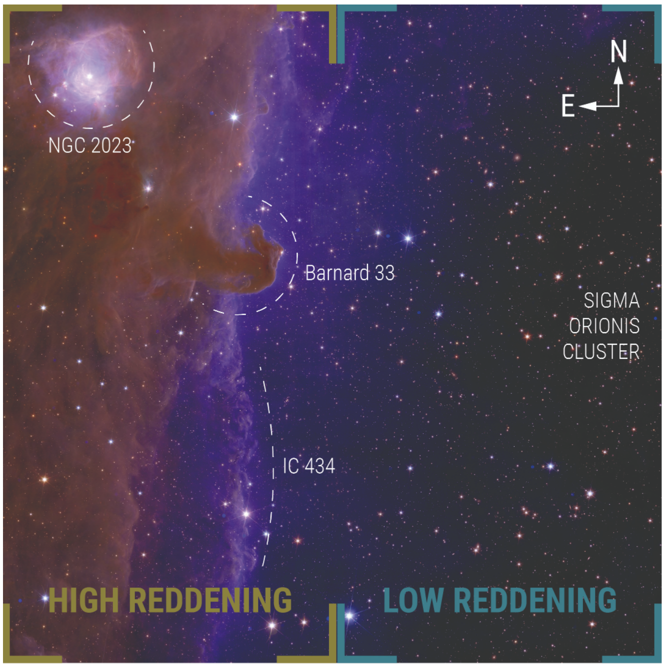


**Fig. 1.** Multi-colour mosaic of the *Euclid* pointing studied in this work. The area covers 0.58 square degrees. The dark neck of the Horsehead points towards the bright $\sigma$ Orionis star that is located just outside the field of view. The bright nebular emission crossing the image is the IC 434 H II region, and the bright concentration in the upper left corner is NGC 2023. This paper focuses on the low-reddening part of the field of view that was cleared out by the hot $\sigma$ Orionis star.

the gaps between the detectors can be covered when a stack of the four images is made. However, due to a failure in the implementation of the dithering during the science-verification phase, the pattern was not optimised, and there are some gaps in the mosaic of this ERO footprint. Furthermore, during the data processing, it was realised that about 5% of the FoV was covered by only one image and that cosmic rays could not be removed efficiently. After data reduction and image stacking, following the procedures described in Cuillandre et al. (2025), the data were validated and considered ready for scientific exploitation. In this work, the catalogues and images of the ERO public data release are used (Euclid Early Release Observations 2024). They do not include any spectroscopic data.

## 3. Region covered in the early release observation

The ERO pointing shown in Fig. 1 contains the complex region created by the interaction between the hot $\sigma$ Orionis star and the Orion B giant molecular cloud (Lynds 1630). Extreme ultraviolet radiation from the O-type star $\sigma$ Orionis creates a bright ionisation front that is known as the IC 434 H II region. A complicated pattern of bright and dark regions is clearly seen in fine detail in the *Euclid* mosaic (Fig. 1). The Horsehead nebula is projected in the foreground of the H II region at a distance of about 360 pc, and it points towards the ionising $\sigma$ Orionis star that is in the background (Bally et al. 2018). Another ionisation source in the ERO-SOri FoV is the B-type star HD 37903, which illuminates a reflection nebula and is associated with the embedded open cluster NGC 2023, which contains very young low-mass stars (Depoy et al. 1990; Mookerjea et al. 2009; Kounkel et al. 2017). As a consequence of the complex previous

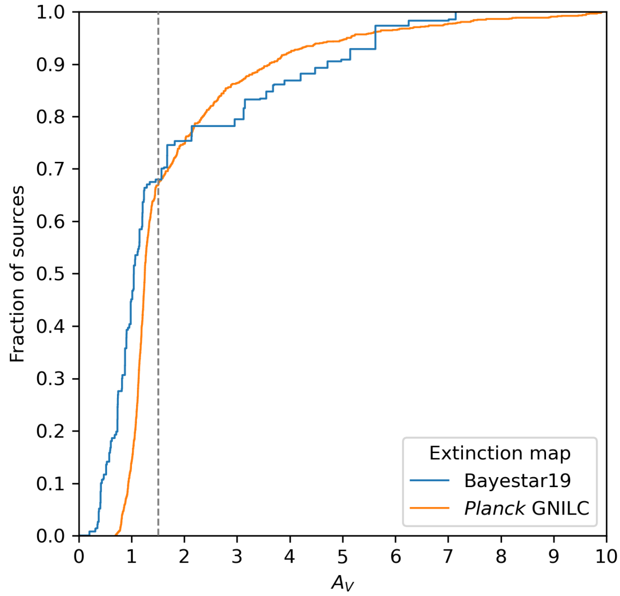


**Fig. 2.** Cumulative distribution of interstellar reddening in the *Euclid* ERO region shown in Fig. 1. Two different methods of estimating the reddening are compared. About 70% of the FoV has a modest reddening of less than 1.7 mag in the visible. This reddening value is used in the reddening vectors shown in the colour–magnitude and colour–colour diagrams of the highly reddened region. This work focuses on the $\sigma$ Orionis cluster, which is located in the low-reddening region of the FoV.

and ongoing star-formation processes, there are patches with significant interstellar reddening. The $A_V$ extinction values for all the sources identified in this ERO pointing were calculated with two extinction maps from the literature: the generalised needlet internal linear combination map from Planck Collaboration Int. XLVIII (2016), which is a 2D extinction map, and the 3D extinction map Bayestar19 (Green 2018; Green et al. 2019), for which we assumed a mean distance of 400 pc to the Orion star-forming region. Both extinction maps were queried with the `dustmap`[1] package. The cumulative distribution function of the $A_V$ extinction of our sources is shown in Fig. 2. The two extinction maps agree quite well and show that about 70% of the sources in the FoV have $A_V$ values between 0 and 1.7 mag. In the future, we plan to use more specific methods that take the extinction of the individual sources into account (e.g., Olivares et al. 2021).

## 4. *Euclid* view of the $\sigma$ Orionis substellar members

The *Euclid* footprint of the ERO pointing includes a portion of the well-known $\sigma$ Orionis cluster, which has been a favourite hunting ground for very young substellar objects and FFPs for over two decades (Zapatero Osorio et al. 2000; Damian et al. 2023). A review of the $\sigma$ Orionis cluster properties was provided by Walter et al. (2008). A recent assessment of cluster membership using the *Gaia* third data release (DR3, Gaia Collaboration 2023) has been carried out in a study of the young populations in the region (Žerjal et al. 2024). The ages of most $\sigma$ Orionis cluster members are in the range from 1 Myr to 5 Myr (Zapatero Osorio et al. 2002). We adopted an age of (3 ± 2) Myr and a distance of 402.7±9.0 pc (Žerjal et al. 2024) for the $\sigma$ Orionis cluster. The deepest survey carried out to date

[1] https://dustmaps.readthedocs.io/en/latest/index.html

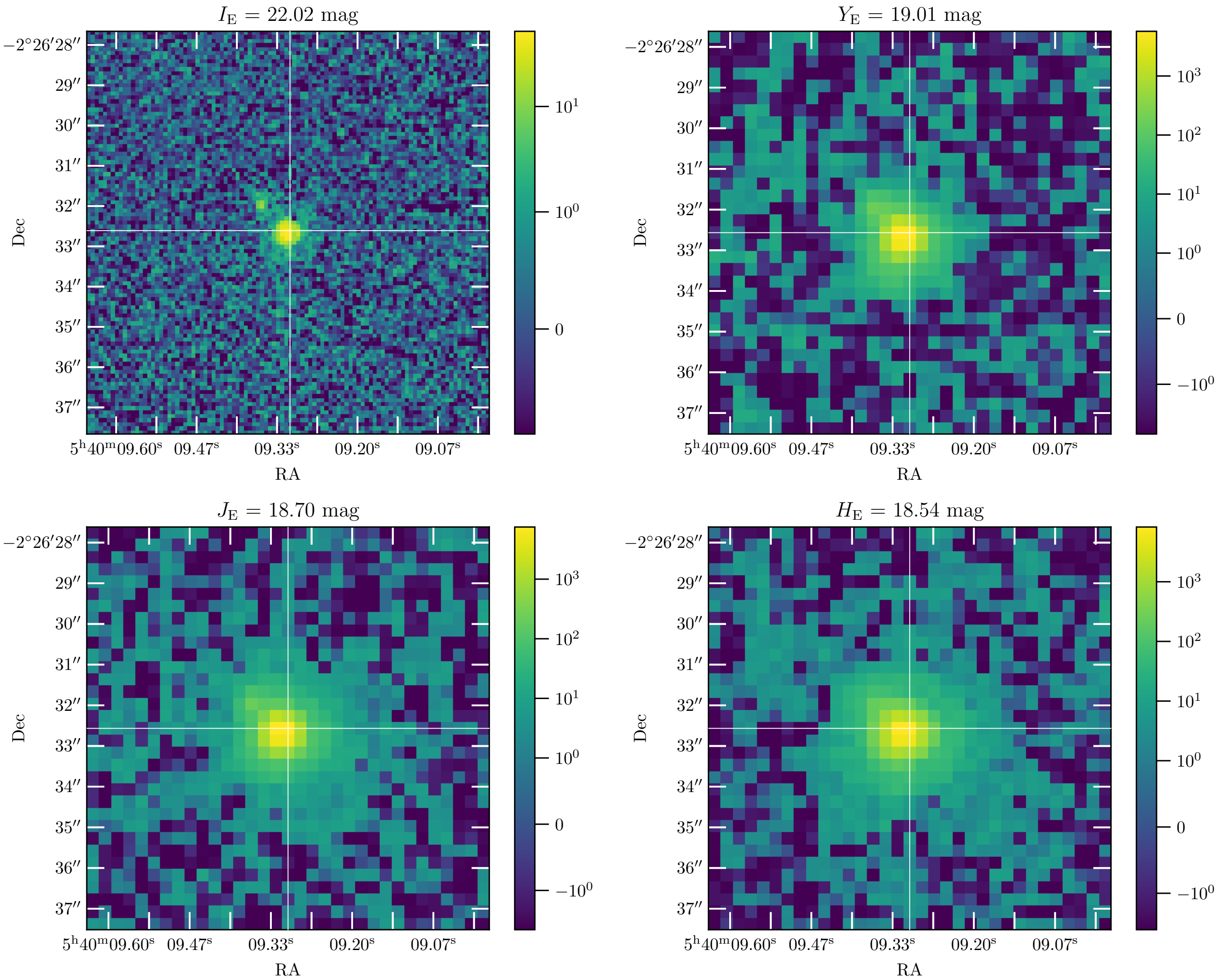


**Fig. 3.** Mosaic of *Euclid* images centred on the benchmark object S Ori 52 in the four different photometric passbands. A clearly resolved visual companion is visible in the VIS image.

in the search for FFPs belonging to $\sigma$ Orionis was reported by Peña Ramírez et al. (2012) using ground-based telescopes.

### 4.1. Definition of benchmarks for Euclid based on confirmed $\sigma$ Orionis substellar objects

We selected seven confirmed very cool members of the $\sigma$ Orionis cluster with a ground-based low-resolution optical and near-infrared spectroscopic classification. Their names and coordinates are listed in Table A.1, together with the spectral types from the literature (Zapatero Osorio et al. 2000; Barrado y Navascués et al. 2001; Martín et al. 2001; Zapatero Osorio et al. 2017). The parameters of these seven benchmarks in the *Euclid* ERO catalogue are provided in Table A.2.

The values of the SPREAD_MODEL parameter for the benchmarks in all the *Euclid* passbands deviate very little from zero, as expected for bona fide point sources. This parameter was developed as a star and galaxy classifier by the data-management pipeline of the Dark Energy Survey (Mohr et al. 2012), and it was shown to be a good discriminant for point sources in nearby young clusters and stellar associations (Bouy et al. 2013). The parameter was adopted as one of the main selection criteria to separate point sources from galaxies.

We note that two benchmarks, namely S Ori 52 and 60, have slightly higher FWHM_IMAGE_I values in the ERO catalogue than the other four benchmarks, suggesting that they might be binaries with an angular separation close to the limit of the spatial resolution of the VIS data. Moreover, a resolved faint visual companion was spotted close to S Ori 52 at position J054009.36−022631.93 in the VIS image (see Fig. 3). S Ori 52 has an optical spectral type of L0.5 and a mass of about 15 $M_{\rm J}$ (Béjar et al. 2001). The candidate wide companion to S Ori 52 is 3.2 mag fainter in the $I_{\rm E}$ passband than the primary, the angular separation is 0.96″ (387 au at 403 pc), and the position angle is 43.3°. The pair is barely resolved in the NISP images because they have a lower spatial resolution than the VIS image. Using PSF photometry, the difference in magnitude in the $J_{\rm E}$ passband is 3.96. This difference is larger than in $I_{\rm E}$, indicating that the companion has a slightly bluer $I_{\rm E}$–$J_{\rm E}$ colour than the primary, and casting some doubt on the physical association of these two objects. The possibility that *Euclid* may have found two substellar binaries close to the angular resolution of the VIS images in a sample of only seven benchmarks in the $\sigma$ Orionis cluster is interesting and deserves further scrutiny. A Hubble Space Telescope (HST) imaging survey of wide binaries (projected semi-major axes between 100 and 1000 au) among pre-main-sequence (PMS) stars in the Orion star-forming complex found a binary frequency of $12.5^{+1.2}_{-0.8}$% (Kounkel et al. 2016), and recent work with the *James Webb* Space Telescope (JWST) suggested that substellar-mass binaries in the Trapezium cluster could be common (McCaughrean & Pearson 2023). On the other hand, no resolved binaries with separations >20 au were found in an imaging survey of 33 BDs in two young open clusters (ages in the range from 70 to 120 Myr) that was carried out with the HST (Martín et al. 2003).

### 4.2. Contamination estimates and definition of selection cuts for the Euclid data

To assess the likelihood that the substellar object candidates are contaminated by background extragalactic objects and by foreground ultracool dwarfs, all the objects that were not saturated in the *Euclid* images and listed by Peña Ramírez et al. (2012) in the ERO-SOri FoV were visually inspected in the VIS and NISP images and were cross-correlated with the ESO VISTA Hemisphere Survey (VHS) catalogue (McMahon et al. 2021) to check for proper motions. The total proper motion of true cluster members is expected to be ≤20 mas per year and thus should not be measurable when comparing VHS and NISP data. A summary of the results of this contamination assessment is provided in Table A.3. Sources that are spatially resolved as extended objects in any of the *Euclid* passbands are considered as non-members. They have values of the FWHM and SPREAD_MODEL parameters larger than those of the benchmarks. Sources that are detected to move by ≥100 mas from the VHS epoch to the *Euclid* epoch (baseline 14 years) are classified as non-members and are labelled as high proper motion. In particular, the *Euclid* VIS spatial resolution has been crucial to show that some of the very faint and red sources identified in Peña Ramírez et al. (2012) are likely to be galaxies. For the benchmarks, we confirmed that their coordinates match those from the VHS catalogue within 100 mas. As expected, the most frequent contamination comes from extended objects that are probably background galaxies (9/38 or 24%), particularly at the faint end of the sample. The ratio of extragalactic sources to ultracool dwarfs is expected to increase with increasing depth. It has recently been reported from JWST Near-Infrared Spectrograph spectroscopic follow-up of photometrically selected JWST Near-Infrared Camera compact sources that the ratio of extragalactic objects and ultracool dwarfs is 11/3 at depths fainter than those reached by the *Euclid* images (Langeroodi & Hjorth 2023).

The contamination by background extragalactic sources, the inhomogeneous interstellar extinction in star-forming regions, the possible presence of colour excesses owing to discs and accretion activity, and the low surface gravity and extreme youth of FFPs in Orion together make the selection of bona fide substellar objects quite challenging. The *Euclid* passbands are not specifically designed to distinguish FFPs from other types of objects. They are broader than the passbands commonly used in ground-based surveys because they include spectral regions that are affected by saturated telluric water absorption. The calibrations available for this ERO study are scarce. Improved calibrations are expected in the future when *Euclid* photometry and spectroscopy of benchmark ultracool dwarfs become available. We limited the scope of this work to present a high-purity approach to select objects using the *Euclid* ERO catalogue and images that is anchored in the properties of the benchmarks described in the previous section. The selection cuts adopted in this work are presented in Table A.4. To arrive at these selection cuts, we calculated the 1 $\sigma$ dispersion around the mean of the values for the benchmark sources and added it to both extremes of the distribution.

The ERO-SOri photometric catalogue was filtered using the cuts provided in Table A.4. The number of objects left after each step and the percentage with respect to the original sample are also given in the table. The percentage of sources detected in the $J_{\rm E}$ band in the whole FoV is 76.83% of the total number of sources in the ERO catalogue. Sources not detected in the $J_{\rm E}$ band were excluded from this work because young substellar objects are expected to be much brighter in the $J_{\rm E}$ band than in the $I_{\rm E}$ band. The CLASS_STAR classifier was found to be redundant with the SPREAD_MODEL parameter, and the latter was chosen because the values for the benchmarks are more stable. The FoV was divided into two regions separated by a constant RA value of 85.1875°. We call the low-reddening and dark-background part the $\sigma$ Orionis region (RA < 85.1875°) and the high-reddening and bright-background part the Horsehead region. We compared the distribution of SPREAD_MODEL_J between these two parts of the FoV and found that it is narrower in the $\sigma$ Orionis region than in the Horsehead region (Fig. B.1). This is likely due to the influence of a brighter background on the Horsehead side owing to light that is reflected in the nebulosity. Thus, we consider that the cuts defined in this work are valid only for regions with low interstellar background and negligible extinction. For the regions affected by high sky background, it will be important to obtain a new sample of substellar benchmarks using the *Euclid* NISP spectra and to consider the effects of variable background on the PSF of the sources.

### 4.3. Selection of new substellar member candidates in the $\sigma$ Orionis cluster with Euclid data

After applying all the selection cuts defined above, only 2% of the sources in the initial catalogue remained. They are plotted in the $I_{\rm E}$ versus $I_{\rm E}$–$J_{\rm E}$ colour–magnitude diagram (CMD) following the approach of previous searches for substellar objects in the $\sigma$ Orionis region (Peña Ramírez et al. 2012), and were compared with the 3-Myr isochrone provided by the ATMO models of Phillips et al. (2020), which were transformed into the *Euclid* photometric system for this work. These models were tested using the dynamic lithium-boundary method for brown dwarf binaries with dynamical masses and were found to fit the observational data better than other sets of models in the literature (Martín et al. 2022). The *Euclid* data and the CEQ (equilibrium chemistry) ATMO 3-Myr isochrone are shown in the CMD displayed in Fig. 4. The benchmarks clearly define the $\sigma$ Orionis sequence, and other objects in the *Euclid* data that appear to follow this cluster sequence were identified previously as photometric candidate members (Peña Ramírez et al. 2012). Their *Euclid* coordinates and photometry are provided in Table A.5. Seven new objects were found to be located close to the cluster sequence and are well separated from the cloud of background sources, including two very faint objects that extend the sequence to fainter magnitudes than previous surveys. The three brightest objects in the NISP $J_{\rm E}$ band were retrieved in the VHS catalogue, and their coordinates were found to agree within 100 mas. This means that they do not have a high proper motion. The coordinates and photometry of these seven

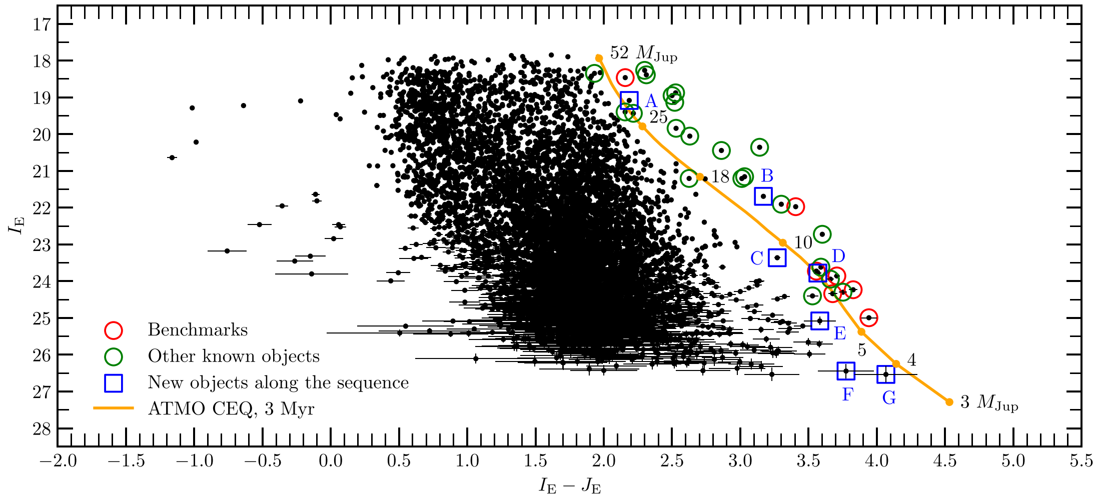


**Fig. 4.** $I_{\rm E}$ vs. $I_{\rm E} - J_{\rm E}$ colour–magnitude diagram for the $\sigma$ Orionis part of the FoV. The black points are all the *Euclid* sources that remain after applying all the cuts. Benchmark objects are denoted with red circles. New objects near the cluster sequence are denoted with blue squares and labelled with capital letters. Known sources other than the benchmarks in the $\sigma$ Orionis cluster are denoted with green circles. An ATMO CEQ isochrone (see Phillips et al. 2020) for an age of 3 Myr and a distance of 402.74 pc is shown. Theoretical masses are labelled on the isochrone.

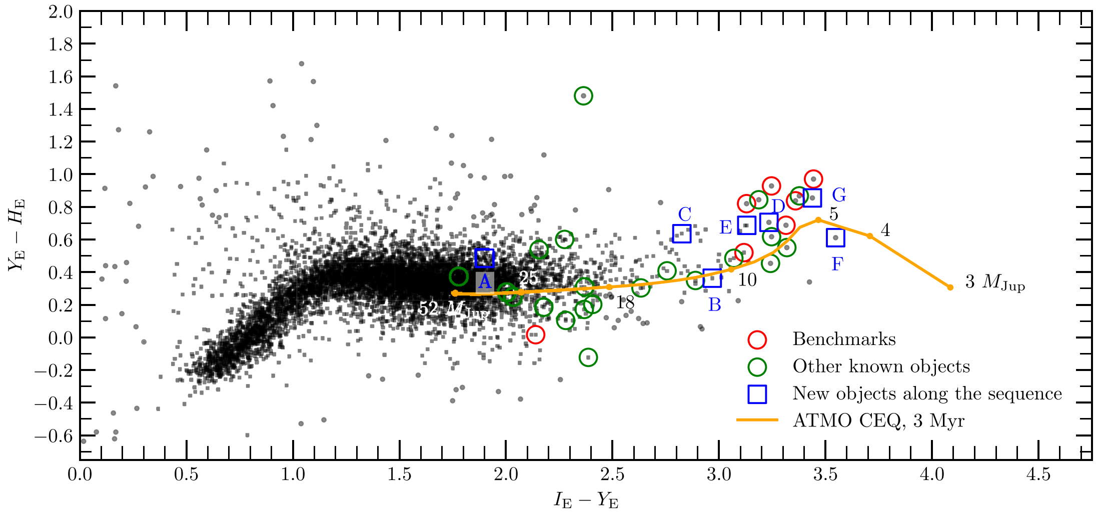


**Fig. 5.** $I_{\rm E}$–$Y_{\rm E}$ vs. $Y_{\rm E}$–$H_{\rm E}$ Colour–colour diagram for the same region as in the previous figure ($\sigma$ Orionis). All the symbols remain the same.

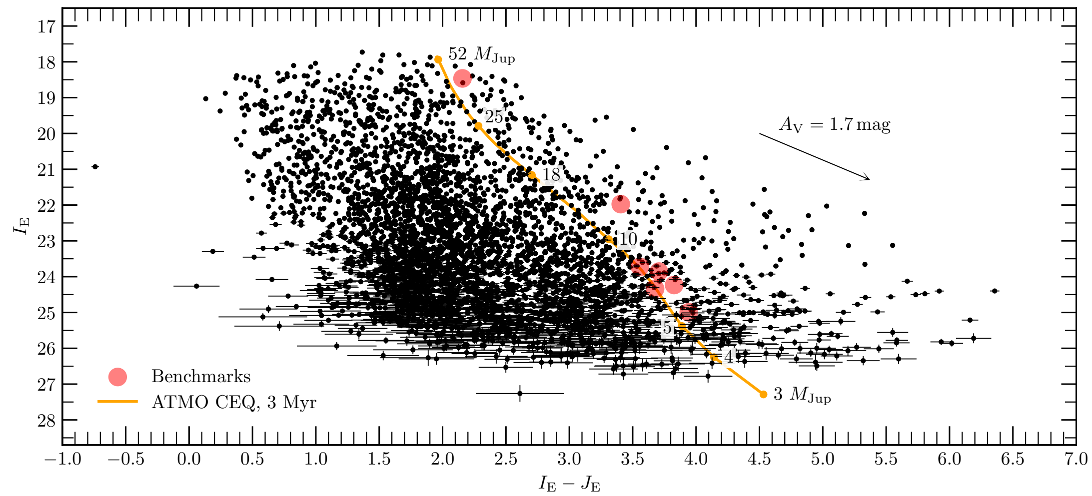


**Fig. 6.** $I_{\rm E}$ vs. $I_{\rm E} - J_{\rm E}$ colour–magnitude diagram for the Horsehead part of the FoV (not $\sigma$ Orionis). The $\sigma$ Orionis benchmarks are denoted with red circles. A reddening vector is shown as an arrow.

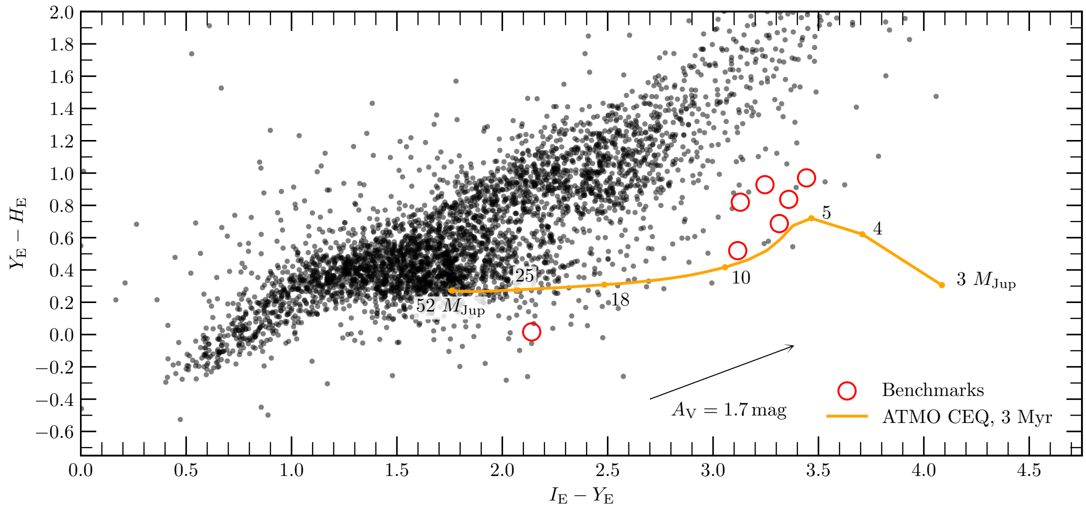


**Fig. 7.** $I_E - Y_E$ vs. $Y_E - H_E$ colour–colour diagram for the Horsehead part of the FoV (not $\sigma$ Orionis). The $\sigma$ Orionis benchmarks are denoted with red circles. A reddening vector is shown as an arrow.

new *Euclid* objects of interest identified in the $\sigma$ Orionis cluster sequence are given in Table A.6.

Further examination of the cluster sequence, its degree of agreement with the ATMO isochrone, and the location of new candidate members was made in the colour–colour diagram shown in Fig. 5. The coolest benchmarks define a well-separated locus away from the cloud of contaminating sources. The behaviour of the benchmarks is qualitatively fairly well reproduced by the isochrone, although quantitatively, the fit could be improved because the isochrone does not reach as large a $Y_E - H_E$ colour as observed. The blueing of the isochrone in the $Y_E - H_E$ colour beyond $I_E - Y_E \geq 3.5$ is an effect of the appearance of methane in the transition from L- to T-type spectra. The new sources with codes D, E, and G fall within the L-type benchmark locus, making them strong FFP candidates. Source F is slightly bluer in $Y_E$–$H_E$ than the faintest benchmark, and it is also closer to the isochrone, suggesting that it might be the first L/T transition FFP identified in the $\sigma$ Orionis cluster. Confirmation of these tentative assessments requires spectroscopy.

To determine the effects of reddening in the selection of substellar candidates, the same cuts as applied to the $\sigma$ Orionis region were also applied to the Horsehead regions. The CMD and colour–colour diagrams are shown in Figs. 6 and 7, respectively. The separation between the cluster sequence defined by the benchmarks and the cloud of sources is no longer well defined in the CMD, and the locus of benchmarks in the colour–colour diagram is not well isolated. This example shows that it is difficult to select substellar candidates in regions with high interstellar reddening. Future work will address this issue.

To search for binaries, we show in Fig. B.2 the FWHM values (in pixels) versus aperture magnitudes measured in the VIS images for all the objects under study (benchmarks, confirmed candidates in the cluster sequence, and new discoveries). In addition to the two binary candidates among the benchmarks, one more candidate is found among the confirmed objects and another among the new objects that were found with *Euclid*. The object labelled G could be the first $\sigma$ Orionis counterpart to the Jupiter-mass binary candidates reported in the Trapezium cluster (McCaughrean & Pearson 2023), but it needs confirmation with higher spatial resolution images that might be provided by HST optical or JWST near-infrared imaging observations.

## 5. *Euclid* substellar initial mass function of the $\sigma$ Orionis cluster

Our results are used here to revise the very low mass IMF of the $\sigma$ Orionis cluster and try to extend it deeper into the planetary-mass regime. The *Gaia* sample covers the domain of very low mass stars and *Euclid* provides a continuation into the substellar-mass regime, reaching down to about 4 $M_J$.

The mass-luminosity relation from the 3 Myr ATMO CEQ models was used for the substellar domain. The PAdova and TRieste Stellar Evolution Code (PARSEC) models (Bressan et al. 2012; Pastorelli et al. 2020) were used for the stellar domain. The IMF of the $\sigma$ Orionis cluster using the *Gaia*-DR3 membership study by Žerjal et al. (2024), combined with the results of this work, is displayed in Fig. 8. Our results are consistent with a multi-power-law distribution for the IMF.

A comprehensive study of the IMF within a distance of 20 pc from the Sun has reported a change in the slope in the substellar domain (Kirkpatrick et al. 2024). The authors claimed that the solar vicinity IMF can be expressed as $dN/dM = C\,M^{-\alpha}$ with four different values of the power-law exponent for different mass intervals. In particular, we are concerned with the low-mass tail of the IMF, where the slope estimated by Kirkpatrick et al. (2024) steepens from a value of $\alpha = 0.25$ in the mass range $0.05\,M_\odot < M < 0.22\,M_\odot$ to $\alpha = 0.60$ in the mass range $0.01\,M_\odot < M < 0.05\,M_\odot$.

We identified three different mass regimes here: the very low mass stellar domain from 0.15 to 0.1 $M_\odot$ with $\alpha = 0.26\pm0.10$, the brown dwarf domain from 0.1 to 0.011 $M_\odot$ with $\alpha = 0.18\pm0.01$, and the planetary-mass domain from 0.011 to 0.003 $M_\odot$ with $\alpha = 0.12\pm0.02$. These values were obtained with the linear fits that are shown in Fig. 8. We excluded from the fits the mass range between 0.1 $M_\odot$ and 0.05 $M_\odot$ because these objects are too faint to be complete for Gaia and too bright for *Euclid*. The error bars quoted for the IMF slopes were estimated by simulations of the effects of age, distance, and photometric uncertainties.

Our $\sigma$ Orionis IMF results are consistent with the field in the very low mass stellar regime and extend deeper into the substellar regime than the field IMF. We do not confirm a steepening of the substellar IMF at the planetary-mass end. The slope of our IMF in the substellar regime is shallower than that reported in the previous study of the $\sigma$ Orionis cluster by Peña Ramírez et al.

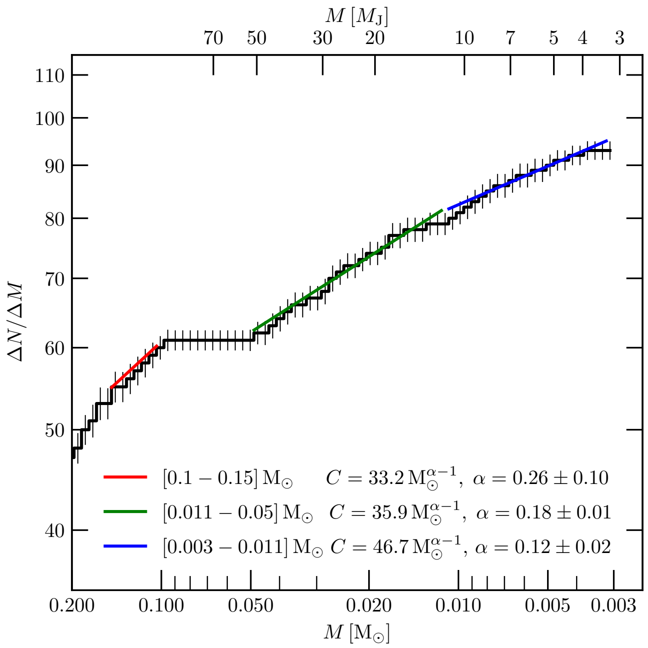


**Fig. 8.** Combined very low mass *Euclid–Gaia* IMF of the $\sigma$ Orionis cluster with linear fits in three different mass regions.

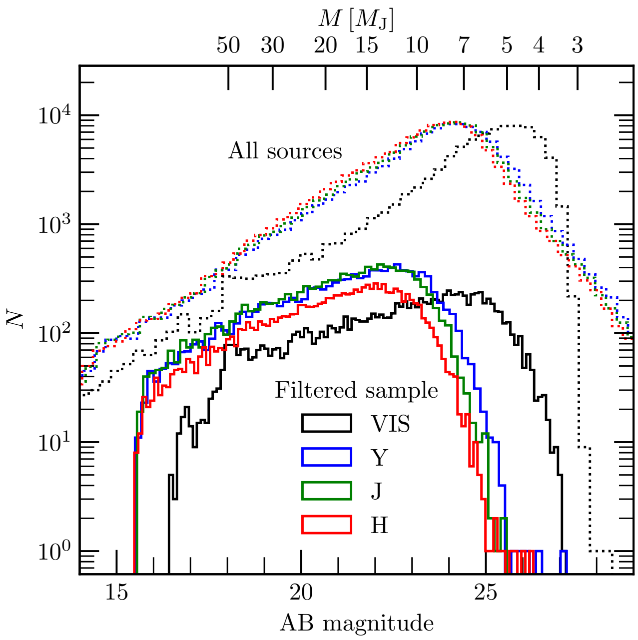


**Fig. 9.** Number counts of *Euclid* sources in the catalogue of the $\sigma$ Orionis region before and after filtering. The correspondence between VIS magnitudes and masses has been made using the ATMO 3 Myr isochrone.

(2012) and also shallower than the IMF study of the solar vicinity by Kirkpatrick et al. (2024), but it is unclear if the difference is significant because there are uncertainties that have not been included in this study. The error bars quoted in our IMF determination only take the internal uncertainty into account when the data were fit with power laws. The comparisons between different substellar IMFs are affected by low number statistics and other uncertainties (e.g. unresolved binaries and mass determination using evolutionary models), particularly at the planetary-mass end. The census of directly imaged FFPs must be increased significantly to investigate the possibility of substellar IMF variations in different environments that could be an indication of specific formation pathways in the planetary-mass domain. These results demonstrate that *Euclid* can play a significant role in the detailed study of the low-mass shape of the IMF, and particularly in shedding light on the formation mechanisms of FFPs. Detailed theoretical models developed by different groups have indicated that the shape of the IMF is a useful indicator of the dominant mode of star formation in a given region (Adams & Fatuzzo 1996; Chabrier 2005; Thies et al. 2015), and that a multi-power-law IMF could arise from the interplay between the mass- and time-dependence of exponential growth in a distribution of accreting protostars (Essex et al. 2020).

The photometric completeness of the *Euclid* substellar IMF of the $\sigma$ Orionis cluster was assessed using the source number count distribution shown in Fig. 9. Before any filtering of the catalogue, the depth reached with the VIS instrument indicated that the *Euclid* survey provides a complete detection of objects down to a VIS magnitude of about 27 and to NISP magnitudes of about 25. These values are consistent with the $5\sigma$ values provided by the ERO study of extragalactic fields (Atek et al. 2025). This photometric depth corresponds to 4 $M_J$ for the age and distance of the $\sigma$ Orionis cluster; but after all the filtering needed to select bona fide point sources, the number of objects retained in VIS started to decline at a VIS magnitude of 25, corresponding to masses of about 6 $M_J$. From these considerations, we estimate that the *Euclid* substellar IMF completeness limit of this work is located at 6 $M_J$, and the detection limit is at 4 $M_J$ for the $\sigma$ Orionis cluster.

The substellar IMF presented here does not take the likely presence of unresolved binaries in our sample into account. To assess the impact of unresolved binaries in our study, we generated random simulations of binaries with a frequency of 20% of equal-mass systems. In the Pleiades cluster, the substellar binary frequency with a semimajor axis in the range 7 to 12 au and mass ratios higher than 0.7 was estimated to be up to 20% in a survey carried out with the HST (Martín et al. 2003). A population of binaries in the $\sigma$ Orionis cluster like this would remain unresolved with *Euclid*. We recalculated the IMF for each random simulation of unresolved binaries. The average IMF resulting from ten simulations is shown in Fig. B.3. The main effect is that the slopes of the linear fits become steeper because there are more substellar objects in the sample and their masses tend to be lower than the unresolved binary system masses.

We note that both the photometric uncompleteness of the sample after filtering and the effects of unresolved binaries together contribute to our underestimating of the number of FFPs in our study, particularly at the low-mass end below 6 $M_J$. We therefore consider our conclusion to be solid that there is no evidence for an IMF cutoff down to the detection limit of this study at 4 $M_J$.

## 6. Final remarks: Impact of *Euclid* on the study of free-floating planets in star-forming regions

This work is a showcase of the power of the *Euclid* mission to provide the area and depth required to explore the very low mass population, including FFPs of nearby star-forming regions and very young open clusters. In particular, for the well-known $\sigma$ Orionis cluster, we showed that the sensitivity of the *Euclid* images is capable of probing down to FFPs that could have masses as low as 4 $M_J$ according to theoretical models (for 3 Myr ages) and at a distance of 400 pc. This potential could be compromised by severe contamination from numerous background extragalactic sources if we were not to use stringent selection procedures. Using the *Euclid* data for seven benchmark objects in $\sigma$ Orionis, we developed a high-purity method to filter out the contamination. This method is valid for regions of low reddening, but it needs additional work to be generalised to regions with any reddening. We note that the *Euclid* NISP spectra will likely play an important role in this effort. The ERO images, catalogues, and spectra processed with the official pipeline are planned to be released in March 2025 and they will enable a reassessment of the results presented here. Furthermore, deeper observations of another region in Orion will be made available to the community. Additionally multi-epoch observations with *Euclid* during the lifetime of the mission, possibly filling gaps in the cosmological surveys, can enable the study of proper motions and photometric variability that are useful probes for the study of the low-mass population in star-forming regions.

This paper is a showcase of the potential of *Euclid* to explore nearby star-forming regions. The observations presented here provide a first glimpse of the power of *Euclid* to shed light on the long-standing question of the putative low-mass cutoff of the IMF predicted a long time ago by the theory of opacity-limited fragmentation and collapse of molecular clouds. Our IMF for the $\sigma$ Orionis open cluster extends previous studies to lower planetary masses and suggests that there is no indication that the predicted cutoff at the low-mass end is near the *Euclid* detection limit. Another open question that could be addressed in the future with *Euclid* is the degree of universality of the IMF slope in the planetary-mass regime when comparing different young open clusters, star-forming regions and the field. This work demonstrated the great potential of *Euclid* to determine the substellar IMF down to the FFP regime in nearby star-forming regions and very young open clusters, and it also paves the way to overcome the difficulties associated with the study of very young regions with deep and wide optical and near-infrared space-based imaging observations.

*Acknowledgements.* This work has made use of the Early Release Observations (ERO) data from the *Euclid* mission of the European Space Agency (ESA), 2024. We thank I. Baraffe and M. Phillips for making available a digitised version of their isochrones in the *Euclid* passbands and the referee (Joao Alves) for insightful comments that helped us to improve the manuscript. ELM., MŽ, AE, CDT, SMT, NS, ST, and NV are supported by the European Research Council Advanced grant SUBSTELLAR, project number 101054354. This research has made use of the Spanish Virtual Observatory (`https://svo.cab.inta-csic.es`) project funded by MCIN/AEI/10.13039/501100011033/ through grant PID2020-112949GB-I00 at Centro de Astrobiología (CSIC-INTA). DB and NH have been supported by PID2019-107061GB-C61 by the same agency. PMB is funded by Instituto Nacional de Técnica Aeroespacial through grant PRE-OVE. PC acknowledges financial support from the Spanish Virtual Observatory project (grant PID2020-112949GB-I00). NPB is funded by Vietnam National Foundation for Science and Technology Development (NAFOSTED) under grant number 103.99-2020.63. NL and VJSB acknowledge financial support from the Agencia Estatal de Investigación (AEI/10.13039/501100011033) of the Ministerio de Ciencia e Innovación and the ERDF 'A way of making Europe' through project PID2022-137241NB-C1. CdB acknowledges support from a Beatriz Galindo senior fellowship (BG22/00166) from the Spanish Ministry of Science, Innovation and Universities. AA acknowledges support from the Light Bridges Corporation. The Euclid Consortium acknowledges the European Space Agency and a number of agencies and institutes that have supported the development of *Euclid*, in particular the Agenzia Spaziale Italiana, the Austrian Forschungsförderungsgesellschaft funded through BMK, the Belgian Science Policy, the Canadian Euclid Consortium, the Deutsches Zentrum für Luft- und Raumfahrt, the DTU Space and the Niels Bohr Institute in Denmark, the French Centre National d'Etudes Spatiales, the Fundação para a Ciência e a Tecnologia, the Hungarian Academy of Sciences, the Ministerio de Ciencia, Innovación y Universidades, the National Aeronautics and Space Administration, the National Astronomical Observatory of Japan, the Netherlandse Onderzoekschool Voor Astronomie, the Norwegian Space Agency, the Research Council of Finland, the Romanian Space Agency, the State Secretariat for Education, Research, and Innovation (SERI) at the Swiss Space Office (SSO), and the United Kingdom Space Agency. A complete and detailed list is available on the *Euclid* web site (`http://www.euclid-ec.org`).

## References


Adams, F. C., & Fatuzzo, M. 1996, ApJ, 464, 256
Atek, H., Gavazzi, R., Weaver, J. R., et al. 2025, A&A, 697, A15 (*Euclid* on Sky SI)
Bally, J., Chambers, E., Guzman, V., et al. 2018, AJ, 155, 80
Barrado y Navascués, D., Zapatero Osorio, M. R., Béjar, V. J. S., et al. 2001, A&A, 377, L9
Bayo, A., Barrado, D., Stauffer, J., et al. 2011, A&A, 536, A63
Béjar, V. J. S., Martín, E. L., Zapatero Osorio, M. R., et al. 2001, ApJ, 556, 830
Bodenheimer, P. 1966, ApJ, 144, 103
Bouy, H., Bertin, E., Moraux, E., et al. 2013, A&A, 554, A101
Bouy, H., Tamura, M., Barrado, D., et al. 2022, A&A, 664, A111
Bressan, A., Marigo, P., Girardi, L., et al. 2012, MNRAS, 427, 127
Chabrier, G. 2005, in Astrophysics and Space Science Library, 327, The Initial Mass Function 50 Years Later, eds. E. Corbelli, F. Palla, & H. Zinnecker, 41
Chabrier, G., Baraffe, I., Allard, F., & Hauschildt, P. 2000, ApJ, 542, L119
Chauvin, G., Lagrange, A. M., Dumas, C., et al. 2005, A&A, 438, L25
Chiang, P., & Chen, W. P. 2015, ApJ, 811, L16
Cuillandre, J.-C., Bertin, E., Bolzonella, M., et al. 2025, A&A, 697, A6 (*Euclid* on Sky SI)
Damian, B., Jose, J., Biller, B., et al. 2023, ApJ, 951, 139
Depoy, D. L., Lada, E. A., Gatley, I., & Probst, R. 1990, ApJ, 356, L55
Esplin, T. L., & Luhman, K. L. 2017, AJ, 154, 134
Esplin, T. L., & Luhman, K. L. 2019, AJ, 158, 54
Essex, C., Basu, S., Prehl, J., & Hoffmann, K. H. 2020, MNRAS, 494, 1579
Euclid Collaboration (Scaramella, R., et al.) 2022, A&A, 662, A112
Euclid Collaboration (Cropper, M. S., et al.) 2025, A&A, 697, A2 (*Euclid* on Sky SI)
Euclid Collaboration (Jahnke, K., et al.) 2025, A&A, 697, A3 (*Euclid* on Sky SI)
Euclid Collaboration (Mellier, Y., et al.) 2025, A&A, 697, A1 (*Euclid* on Sky SI)
Euclid Early Release Observations 2024, `https://doi.org/10.57780/esa-qmocze3`
Gaia Collaboration (Vallenari, A., et al.) 2023, A&A, 674, A1
Gauza, B., Béjar, V. J. S., Pérez-Garrido, A., et al. 2015, ApJ, 804, 96
Green, G. M. 2018, J. Open Source Softw., 3, 695
Green, G. M., Schlafly, E., Zucker, C., Speagle, J. S., & Finkbeiner, D. 2019, ApJ, 887, 93
Hennebelle, P., & Chabrier, G. 2008, ApJ, 684, 395
Hunt, L. K., Annibali, F., Cuillandre, J.-C., et al. 2025, A&A, 697, A9 (*Euclid* on Sky SI)
Kirkpatrick, J. D., Marocco, F., Gelino, C. R., et al. 2024, ApJS, 271, 55
Kluge, M., Hatch, N. A., Montes, M., et al. 2025, A&A, 697, A13 (*Euclid* on Sky SI)
Koshimoto, N., Sumi, T., Bennett, D. P., et al. 2023, AJ, 166, 107
Kounkel, M., Megeath, S. T., Poteet, C. A., Fischer, W. J., & Hartmann, L. 2016, ApJ, 821, 52
Kounkel, M., Hartmann, L., Mateo, M., & Bailey, John I., I. 2017, ApJ, 844, 138
Langeroodi, D., & Hjorth, J. 2023, ApJ, 957, L27
Laureijs, R., Amiaux, J., Arduini, S., et al. 2011, arXiv e-prints [arXiv:`1110.3193`]
Lodieu, N., Zapatero Osorio, M. R., Rebolo, R., Martín, E. L., & Hambly, N. C. 2009, A&A, 505, 1115
Lodieu, N., Zapatero Osorio, M. R., Béjar, V. J. S., & Peña Ramírez, K. 2018, MNRAS, 473, 2020
Lodieu, N., Hambly, N. C., & Cross, N. J. G. 2021, MNRAS, 503, 2265
Lucas, P. W., & Roche, P. F. 2000, MNRAS, 314, 858
Lucas, P. W., Roche, P. F., Allard, F., & Hauschildt, P. H. 2001, MNRAS, 326, 695
Lucas, P. W., Weights, D. J., Roche, P. F., & Riddick, F. C. 2006, MNRAS, 373, L60
Luhman, K. L., Peterson, D. E., & Megeath, S. T. 2004, ApJ, 617, 565
Marleau, F. R., Cuillandre, J.-C., Cantiello, M., et al. 2025, A&A, 697, A12 (*Euclid* on Sky SI)
Martín, E. L., Zapatero Osorio, M. R., Barrado y Navascués, D., Béjar, V. J. S., & Rebolo, R. 2001, ApJ, 558, L117
Martín, E. L., Barrado y Navascués, D., Baraffe, I., Bouy, H., & Dahm, S. 2003, ApJ, 594, 525
Martín, E. L., Zhang, J. Y., Esparza, P., et al. 2021, A&A, 655, A3
Martín, E. L., Lodieu, N., & del Burgo, C. 2022, MNRAS, 510, 2841
Martin, E. L., Bouy, H., Martin, D., et al. 2023, Proc., 30th Rencontres du Vietnam: Windows on the Universe

Massari, D., Dalessandro, E., Erkal, D., et al. 2025, A&A, 697, A8 (*Euclid* on Sky SI)
McCaughrean, M. J., & Pearson, S. G. 2023, A&A, submitted [arXiv:2310.03552]
McMahon, R. G., Banerji, M., Gonzalez, E., et al. 2021, VizieR Online Data Catalog, II/367
Miret-Roig, N. 2023, Ap&SS, 368, 17
Miret-Roig, N., Bouy, H., Raymond, S. N., et al. 2022, Nat. Astron., 6, 89
Mohr, J. J., Armstrong, R., Bertin, E., et al. 2012, SPIE Conf. Ser., 8451, 84510D
Mondal, A., & Chattopadhyay, T. 2019, New A, 66, 45
Mookerjea, B., Sandell, G., Jarrett, T. H., & McMullin, J. P. 2009, A&A, 507, 1485
Mróz, P., Ryu, Y. H., Skowron, J., et al. 2018, AJ, 155, 121
Oasa, Y., Tamura, M., & Sugitani, K. 1999, ApJ, 526, 336
Olivares, J., Bouy, H., Sarro, L. M., et al. 2021, A&A, 649, A159
Padoan, P., & Nordlund, Å. 2004, ApJ, 617, 559
Pastorelli, G., Marigo, P., Girardi, L., et al. 2020, MNRAS, 498, 3283
Peña Ramírez, K., Béjar, V. J. S., Zapatero Osorio, M. R., Petr-Gotzens, M. G., & Martín, E. L. 2012, ApJ, 754, 30
Phillips, M. W., Tremblin, P., Baraffe, I., et al. 2020, A&A, 637, A38
Planck Collaboration Int. XLVIII. 2016, A&A, 596, A109
Saifollahi, T., Voggel, K., Lançon, A., et al. 2025, A&A, 697, A10 (*Euclid* on Sky SI)
Salpeter, E. E. 1955, ApJ, 121, 161
Scholz, A., Muzic, K., Jayawardhana, R., Almendros-Abad, V., & Wilson, I. 2023, AJ, 165, 196
Silk, J. 1977, ApJ, 214, 152
Solano, E., Gálvez-Ortiz, M. C., Martín, E. L., et al. 2021, MNRAS, 501, 281
Spezzi, L., Petr-Gotzens, M. G., Alcalá, J. M., et al. 2015, A&A, 581, A140
Stahler, S. W. 1988, ApJ, 332, 804
Sumi, T., Koshimoto, N., Bennett, D. P., et al. 2023, AJ, 166, 108
Thies, I., Pflamm-Altenburg, J., Kroupa, P., & Marks, M. 2015, ApJ, 800, 72
Walter, F. M., Sherry, W. H., Wolk, S. J., & Adams, N. R. 2008, in Handbook of Star Forming Regions, Volume I, 4, ed. B. Reipurth (ASP Conf. Ser.), 732
Weaver, J. R., Taamoli, S., McPartland, C. J. R., et al. 2025, A&A, 697, A16 (*Euclid* on Sky SI)
Zapatero Osorio, M. R., Béjar, V. J. S., Martín, E. L., et al. 2000, Science, 290, 103
Zapatero Osorio, M. R., Béjar, V. J. S., Pavlenko, Y., et al. 2002, A&A, 384, 937
Zapatero Osorio, M. R., Béjar, V. J. S., & Peña Ramírez, K. 2017, ApJ, 842, 65
Žerjal, M., Martín, E. L., & Pérez-Garrido, A. 2024, A&A, 686, A161
Zhang, Z., Liu, M. C., Best, W. M. J., Dupuy, T. J., & Siverd, R. J. 2021, ApJ, 911, 7
Zhang, J. Y., Lodieu, N., & Martín, E. L. 2024, A&A, 686, A171



[1] Instituto de Astrofísica de Canarias, Calle Vía Láctea s/n, 38204, San Cristóbal de La Laguna, Tenerife, Spain
[2] Departamento de Astrofísica, Universidad de La Laguna, 38206 La Laguna, Tenerife, Spain
[3] Laboratoire d'Astrophysique de Bordeaux, CNRS and Université de Bordeaux, Allée Geoffroy St. Hilaire, 33165 Pessac, France
[4] Institut universitaire de France (IUF), 1 rue Descartes, 75231 Paris Cedex 05, France
[5] Departamento de Física Fundamental. Universidad de Salamanca. Plaza de la Merced s/n, 37008 Salamanca, Spain
[6] Centro de Astrobiología (CAB), CSIC-INTA, ESAC Campus, Camino Bajo del Castillo s/n, 28692 Villanueva de la Cañada, Madrid, Spain
[7] Departamento de Inteligencia Artificial, Universidad Nacional de Educación a Distancia (UNED), c/Juan del Rosal 16, 28040 Madrid, Spain
[8] Departamento Física Aplicada, Universidad Politécnica de Cartagena, Campus Muralla del Mar, 30202 Cartagena, Murcia, Spain
[9] European Space Agency/ESTEC, Keplerlaan 1, 2201 AZ Noordwijk, The Netherlands
[10] Aurora Technology for European Space Agency (ESA), Camino bajo del Castillo, s/n, Urbanizacion Villafranca del Castillo, Villanueva de la Cañada, 28692 Madrid, Spain
[11] Observatoire Astronomique de Strasbourg (ObAS), Université de Strasbourg – CNRS, UMR 7550, Strasbourg, France
[12] Kapteyn Astronomical Institute, University of Groningen, PO Box 800, 9700 AV Groningen, The Netherlands
[13] Université Paris-Saclay, Université Paris Cité, CEA, CNRS, AIM, 91191 Gif-sur-Yvette, France
[14] Max-Planck-Institut für Astronomie, Königstuhl 17, 69117 Heidelberg, Germany
[15] Ohio University, Physics & Astronomy Department,1 Ohio University, Athens, OH 45701, USA
[16] NSF's NOIR, Lab 950 N. Cherry Avenue, Tucson, AZ 85719, USA
[17] Department of Physics, International University, Ho Chi Minh City, Vietnam
[18] Vietnam National University, Ho Chi Minh City, Vietnam
[19] International Space University, 1 rue Jean-Dominique Cassini, 67400 Illkirch-Graffenstaden, France
[20] School of Physics and Astronomy, University of Leicester, University Road, Leicester LE1 7RH, UK
[21] Université de Franche-Comté, Institut UTINAM, CNRS UMR6213, OSU THETA Franche-Comté-Bourgogne, Observatoire de Besançon, BP 1615, 25010 Besançon Cedex, France
[22] INAF-Osservatorio Astrofisico di Torino, Via Osservatorio 20, 10025 Pino Torinese (TO), Italy
[23] School of Physics, Astronomy and Mathematics, University of Hertfordshire, College Lane, Hatfield AL10 9AB, UK
[24] Université Paris-Saclay, CNRS, Institut d'astrophysique spatiale, 91405, Orsay, France
[25] ESAC/ESA, Camino Bajo del Castillo, s/n, Urb. Villafranca del Castillo, 28692 Villanueva de la Cañada, Madrid, Spain
[26] INAF – Osservatorio Astronomico di Brera, Via Brera 28, 20122 Milano, Italy
[27] INAF – Osservatorio di Astrofisica e Scienza dello Spazio di Bologna, Via Piero Gobetti 93/3, 40129 Bologna, Italy
[28] Dipartimento di Fisica e Astronomia, Università di Bologna, Via Gobetti 93/2, 40129 Bologna, Italy
[29] INFN – Sezione di Bologna, Viale Berti Pichat 6/2, 40127 Bologna, Italy
[30] INAF – Osservatorio Astronomico di Padova, Via dell'Osservatorio 5, 35122 Padova, Italy
[31] Centre National d'Etudes Spatiales – Centre spatial de Toulouse, 18 avenue Edouard Belin, 31401 Toulouse Cedex 9, France
[32] Max Planck Institute for Extraterrestrial Physics, Giessenbachstr. 1, 85748 Garching, Germany
[33] Universitäts-Sternwarte München, Fakultät für Physik, Ludwig-Maximilians-Universität München, Scheinerstrasse 1, 81679 München, Germany
[34] Dipartimento di Fisica, Università di Genova, Via Dodecaneso 33, 16146 Genova, Italy
[35] INFN – Sezione di Genova, Via Dodecaneso 33, 16146 Genova, Italy
[36] Department of Physics "E. Pancini", University Federico II, Via Cinthia 6, 80126 Napoli, Italy
[37] INAF – Osservatorio Astronomico di Capodimonte, Via Moiariello 16, 80131 Napoli, Italy
[38] INFN section of Naples, Via Cinthia 6, 80126 Napoli, Italy
[39] Instituto de Astrofísica e Ciências do Espaço, Universidade do Porto, CAUP, Rua das Estrelas, 4150-762 Porto, Portugal
[40] Dipartimento di Fisica, Università degli Studi di Torino, Via P. Giuria 1, 10125 Torino, Italy
[41] INFN – Sezione di Torino, Via P. Giuria 1, 10125 Torino, Italy
[42] INAF – IASF Milano, Via Alfonso Corti 12, 20133 Milano, Italy
[43] Centro de Investigaciones Energéticas, Medioambientales y Tecnológicas (CIEMAT), Avenida Complutense 40, 28040 Madrid, Spain
[44] Port d'Informació Científica, Campus UAB, C. Albareda s/n, 08193 Bellaterra (Barcelona), Spain
[45] Institute for Theoretical Particle Physics and Cosmology (TTK), RWTH Aachen University, 52056 Aachen, Germany
[46] INAF-Osservatorio Astronomico di Roma, Via Frascati 33, 00078 Monteporzio Catone, Italy

[47] Dipartimento di Fisica e Astronomia “Augusto Righi” – Alma Mater Studiorum Università di Bologna, Viale Berti Pichat 6/2, 40127 Bologna, Italy
[48] Institute for Astronomy, University of Edinburgh, Royal Observatory, Blackford Hill, Edinburgh EH9 3HJ, UK
[49] Jodrell Bank Centre for Astrophysics, Department of Physics and Astronomy, University of Manchester, Oxford Road, Manchester M13 9PL, UK
[50] European Space Agency/ESRIN, Largo Galileo Galilei 1, 00044 Frascati, Roma, Italy
[51] Université Claude Bernard Lyon 1, CNRS/IN2P3, IP2I Lyon, UMR 5822, Villeurbanne, 69100, France
[52] Institute of Physics, Laboratory of Astrophysics, Ecole Polytechnique Fédérale de Lausanne (EPFL), Observatoire de Sauverny, 1290 Versoix, Switzerland
[53] UCB Lyon 1, CNRS/IN2P3, IUF, IP2I Lyon, 4 rue Enrico Fermi, 69622 Villeurbanne, France
[54] Mullard Space Science Laboratory, University College London, Holmbury St Mary, Dorking, Surrey RH5 6NT, UK
[55] Departamento de Física, Faculdade de Ciências, Universidade de Lisboa, Edifício C8, Campo Grande, 1749-016 Lisboa, Portugal
[56] Instituto de Astrofísica e Ciências do Espaço, Faculdade de Ciências, Universidade de Lisboa, Campo Grande, 1749-016 Lisboa, Portugal
[57] Department of Astronomy, University of Geneva, ch. d’Ecogia 16, 1290 Versoix, Switzerland
[58] INAF-Istituto di Astrofisica e Planetologia Spaziali, via del Fosso del Cavaliere, 100, 00100 Roma, Italy
[59] INFN-Padova, Via Marzolo 8, 35131 Padova, Italy
[60] Institut d’Estudis Espacials de Catalunya (IEEC), Edifici RDIT, Campus UPC, 08860 Castelldefels, Barcelona, Spain
[61] Institut de Ciencies de l’Espai (IEEC-CSIC), Campus UAB, Carrer de Can Magrans, s/n Cerdanyola del Vallés, 08193 Barcelona, Spain
[62] INAF-Osservatorio Astronomico di Trieste, Via G. B. Tiepolo 11, 34143 Trieste, Italy
[63] Aix-Marseille Université, CNRS/IN2P3, CPPM, Marseille, France
[64] Istituto Nazionale di Fisica Nucleare, Sezione di Bologna, Via Irnerio 46, 40126 Bologna, Italy
[65] FRACTAL S.L.N.E., calle Tulipán 2, Portal 13 1A, 28231 Las Rozas de Madrid, Spain
[66] Dipartimento di Fisica “Aldo Pontremoli”, Università degli Studi di Milano, Via Celoria 16, 20133 Milano, Italy
[67] Institute of Theoretical Astrophysics, University of Oslo, P.O. Box 1029 Blindern, 0315 Oslo, Norway
[68] Leiden Observatory, Leiden University, Einsteinweg 55, 2333 CC Leiden, The Netherlands
[69] Jet Propulsion Laboratory, California Institute of Technology, 4800 Oak Grove Drive, Pasadena, CA, 91109, USA
[70] Department of Physics, Lancaster University, Lancaster, LA1 4YB, UK
[71] Felix Hormuth Engineering, Goethestr. 17, 69181 Leimen, Germany
[72] Technical University of Denmark, Elektrovej 327, 2800 Kgs. Lyngby, Denmark
[73] Cosmic Dawn Center (DAWN), Denmark
[74] Institut d’Astrophysique de Paris, UMR 7095, CNRS, and Sorbonne Université, 98 bis boulevard Arago, 75014 Paris, France
[75] NASA Goddard Space Flight Center, Greenbelt, MD 20771, USA
[76] Department of Physics and Helsinki Institute of Physics, Gustaf Hällströmin katu 2, 00014 University of Helsinki, Finland
[77] AIM, CEA, CNRS, Université Paris-Saclay, Université de Paris, 91191 Gif-sur-Yvette, France
[78] Université de Genève, Département de Physique Théorique and Centre for Astroparticle Physics, 24 quai Ernest-Ansermet, 1211 Genève 4, Switzerland
[79] Department of Physics, PO Box 64, 00014 University of Helsinki, Finland
[80] Helsinki Institute of Physics, Gustaf Hällströmin katu 2, University of Helsinki, Helsinki, Finland
[81] Aix-Marseille Université, CNRS, CNES, LAM, Marseille, France
[82] NOVA optical infrared instrumentation group at ASTRON, Oude Hoogeveensedijk 4, 7991PD, Dwingeloo, The Netherlands
[83] INFN-Sezione di Milano, Via Celoria 16, 20133 Milano, Italy
[84] Universität Bonn, Argelander-Institut für Astronomie, Auf dem Hügel 71, 53121 Bonn, Germany
[85] Dipartimento di Fisica e Astronomia “Augusto Righi" – Alma Mater Studiorum Università di Bologna, via Piero Gobetti 93/2, 40129 Bologna, Italy
[86] Department of Physics, Centre for Extragalactic Astronomy, Durham University, South Road, DH1 3LE, UK
[87] Université Paris Cité, CNRS, Astroparticule et Cosmologie, 75013 Paris, France
[88] University of Applied Sciences and Arts of Northwestern Switzerland, School of Engineering, 5210 Windisch, Switzerland
[89] Institut d’Astrophysique de Paris, 98bis Boulevard Arago, 75014 Paris, France
[90] Institut de Física d’Altes Energies (IFAE), The Barcelona Institute of Science and Technology, Campus UAB, 08193 Bellaterra (Barcelona), Spain
[91] Department of Physics and Astronomy, University of Aarhus, Ny Munkegade 120, 8000 Aarhus C, Denmark
[92] Waterloo Centre for Astrophysics, University of Waterloo, Waterloo, Ontario N2L 3G1, Canada
[93] Department of Physics and Astronomy, University of Waterloo, Waterloo, Ontario N2L 3G1, Canada
[94] Perimeter Institute for Theoretical Physics, Waterloo, Ontario N2L 2Y5, Canada
[95] Space Science Data Center, Italian Space Agency, via del Politecnico snc, 00133 Roma, Italy
[96] Institute of Space Science, Str. Atomistilor, nr. 409 Măgurele, Ilfov, 077125, Romania
[97] Dipartimento di Fisica e Astronomia “G. Galilei”, Università di Padova, Via Marzolo 8, 35131 Padova, Italy
[98] Departamento de Física, FCFM, Universidad de Chile, Blanco Encalada 2008, Santiago, Chile
[99] INFN-Sezione di Roma, Piazzale Aldo Moro 2, c/o Dipartimento di Fisica, Edificio G. Marconi, 00185 Roma, Italy
[100] Satlantis, University Science Park, Sede Bld 48940, Leioa-Bilbao, Spain
[101] Institute of Space Sciences (ICE, CSIC), Campus UAB, Carrer de Can Magrans s/n, 08193 Barcelona, Spain
[102] Infrared Processing and Analysis Center, California Institute of Technology, Pasadena, CA 91125, USA
[103] Instituto de Astrofísica e Ciências do Espaço, Faculdade de Ciências, Universidade de Lisboa, Tapada da Ajuda, 1349-018 Lisboa, Portugal
[104] Universidad Politécnica de Cartagena, Departamento de Electrónica y Tecnología de Computadoras, Plaza del Hospital 1, 30202 Cartagena, Spain
[105] Centre for Information Technology, University of Groningen, PO Box 11044, 9700 CA Groningen, The Netherlands
[106] Institut de Recherche en Astrophysique et Planétologie (IRAP), Université de Toulouse, CNRS, UPS, CNES, 14 Av. Edouard Belin, 31400 Toulouse, France
[107] INFN – Bologna, Via Irnerio 46, 40126 Bologna, Italy
[108] IFPU, Institute for Fundamental Physics of the Universe, via Beirut 2, 34151 Trieste, Italy
[109] INFN, Sezione di Trieste, Via Valerio 2, 34127 Trieste TS, Italy
[110] SISSA, International School for Advanced Studies, Via Bonomea 265, 34136 Trieste TS, Italy
[111] Department of Physics and Astronomy, University of British Columbia, Vancouver, BC V6T 1Z1, Canada

## Appendix A: Tables

**Table A.1.** Benchmark $\sigma$ Orionis cluster members observed with *Euclid*.

| Nickname | RA [hh mm ss.ss] | Dec [deg mm ss.s] | Spectral type |
|---|---|---|---|
| S Ori 28 | 05 39 23.19 | −02 46 55.8 | M5.5 |
| S Ori 52 | 05 40 09.20 | −02 26 32.0 | L0.5 |
| S Ori 60 | 05 39 37.50 | −02 30 42.0 | L2.0 |
| S Ori 62 | 05 39 42.05 | −02 30 31.6 | L4.0 |
| S Ori 054017 | 05 40 17.34 | −02 36 22.6 | L3.5 |
| S Ori 054000 | 05 40 00.04 | −02 40 33.1 | L2.0 |
| S Ori 054037 | 05 40 37.82 | −02 40 01.1 | L4.5 |

**Table A.2.** *Euclid* parameters for $\sigma$ Orionis benchmark objects. FWHM values are given in pixels.

| | Object | | | | | | |
|---|---|---|---|---|---|---|---|
| Parameter | S Ori 28 | S Ori 52 | S Ori 60 | S Ori 62 | S Ori 054017 | S Ori 054000 | S Ori 054037 |
| SPREAD_MODEL_I | $1.20\times10^{-3}$ | $-7.20\times10^{-4}$ | $3.14\times10^{-4}$ | $-7.06\times10^{-4}$ | $2.94\times10^{-3}$ | $1.82\times10^{-3}$ | $1.40\times10^{-3}$ |
| SPREAD_MODEL_Y | $1.24\times10^{-2}$ | $6.25\times10^{-3}$ | $6.96\times10^{-6}$ | $6.61\times10^{-3}$ | $7.24\times10^{-3}$ | $1.48\times10^{-4}$ | $-2.75\times10^{-4}$ |
| SPREAD_MODEL_J | $9.24\times10^{-3}$ | $3.37\times10^{-4}$ | $-1.59\times10^{-3}$ | $-2.14\times10^{-3}$ | $-5.83\times10^{-3}$ | $-1.59\times10^{-4}$ | $-3.76\times10^{-3}$ |
| SPREAD_MODEL_H | $6.80\times10^{-3}$ | $3.26\times10^{-3}$ | $3.74\times10^{-3}$ | $5.47\times10^{-3}$ | $-1.23\times10^{-3}$ | $-4.61\times10^{-3}$ | $1.10\times10^{-2}$ |
| CLASS_STAR_I | 0.98 | 1 | 0.81 | 0.86 | 0.68 | 0.76 | 0.75 |
| CLASS_STAR_Y | 0.99 | 1 | 1 | 0.92 | 0.98 | 0.98 | 1 |
| CLASS_STAR_J | 1 | 1 | 1 | 0.98 | 0.98 | 0.98 | 0.98 |
| CLASS_STAR_H | 1 | 1 | 1 | 0.94 | 0.98 | 0.98 | 0.97 |
| FWHM_IMAGE_I | 1.69 | 2.46 | 2.39 | 1.51 | 1.73 | 1.69 | 1.65 |
| FWHM_IMAGE_Y | 1.44 | 1.52 | 0.78 | 1.78 | 1.61 | 1.59 | 1.42 |
| FWHM_IMAGE_J | 1.83 | 1.54 | 0.8 | 1.46 | 1.29 | 1.66 | 1.37 |
| FWHM_IMAGE_H | 1.79 | 1.56 | 1.69 | 1.89 | 1.64 | 1.4 | 1.56 |
| MAG_AUTO_I | 18.4631 | 21.9735 | 23.7263 | 23.8577 | 24.9944 | 24.2328 | 24.3397 |
| MAGERR_AUTO_I | 0.0005 | 0.0048 | 0.023 | 0.0206 | 0.0537 | 0.0268 | 0.0305 |
| MAG_AUTO_Y | 16.3237 | 18.8565 | 20.597 | 20.5435 | 21.5509 | 20.8739 | 21.0935 |
| MAGERR_AUTO_Y | 0.001 | 0.0035 | 0.012 | 0.0118 | 0.0305 | 0.0215 | 0.0193 |
| MAG_AUTO_J | 16.3058 | 18.5677 | 20.1688 | 20.1503 | 21.0523 | 20.4058 | 20.6629 |
| MAGERR_AUTO_J | 0.0008 | 0.0023 | 0.0068 | 0.007 | 0.0162 | 0.0119 | 0.0111 |
| MAG_AUTO_H | 16.3073 | 18.3369 | 19.7774 | 19.8562 | 20.5806 | 20.0368 | 20.1653 |
| MAGERR_AUTO_H | 0.0008 | 0.002 | 0.0051 | 0.0055 | 0.0121 | 0.0089 | 0.0075 |
| ELLIPTICITY_I | 0.048 | 0.100 | 0.243 | 0.049 | 0.045 | 0.106 | 0.028 |
| ELLIPTICITY_J | 0.017 | 0.049 | 0.023 | 0.04 | 0.07 | 0.107 | 0.062 |

**Table A.3.** *Euclid*-based assessment of previously identified candidate members of the $\sigma$ Orionis cluster and very red sources in the region.

| Name | RA [hh mm ss.ss] | Dec [deg mm ss.s] | Comment |
|---|---|---|---|
| S Ori 69 | 05 39 18.05 | −02 28 54.1 | extended |
| S Ori J053923−021235 | 05 39 23.28 | −02 12 35.0 | extended |
| S Ori J053929−024636 | 05 39 29.36 | −02 46 37.1 | high proper motion |
| S Ori 57 | 05 39 47.05 | −02 25 24.5 | high proper motion |
| S Ori J053956−025315 | 05 39 56.81 | −02 53 14.6 | extended |
| S Ori J054004−025332 | 05 40 04.48 | −02 53 31.9 | extended |
| PBZ2012 J054011−025639 | 05 40 11.62 | −02 56 39.4 | high proper motion |
| S Ori J054014−025146 | 05 40 14.23 | −02 51 46.3 | extended |
| PBZ2012 J054024−024444 | 05 40 24.32 | −02 44 44.3 | extended |
| PBZ2012 J054025−024259 | 05 40 25.39 | −02 42 59.7 | extended |
| PBZ2012 J054026−023100 | 05 40 26.44 | −02 31 00.8 | high proper motion |
| PBZ2012 J054028−025116 | 05 40 27.99 | −02 51 16.7 | extended |
| PBZ2012 J054038−022806 | 05 40 38.42 | −02 28 06.6 | extended |

**Table A.4.** *Euclid* point-source selection criteria applied in this work. The cut in right ascension, RA, divides the area into two parts: the high-reddening region (RA < 85°.1875); and the low reddening region (RA ≥ 85°.1875).

| | | High-reddening region | | Low-reddening region | |
|---|---|---|---|---|---|
| Cut No. | Criteria | Count after cut | % of catalogue | Count after cut | % of catalogue |
| 1 | ra_J_E Cut | 124 249 | 38.04 | 126 693 | 38.79 |
| 2 | −0.011<SPREAD_MODEL_J_E<0.014 | 70 558 | 21.60 | 47 630 | 14.58 |
| 3 | 0.472<FWHM_IMAGE_J_E<2.158 | 24 174 | 7.40 | 14 932 | 4.57 |
| 4 | 0<ELLIPTICITY_J_E<0.138 | 17 423 | 5.33 | 10 742 | 3.29 |
| 5 | −0.01<SPREAD_MODEL_H_E<0.016 | 14 574 | 4.81 | 7944 | 2.97 |
| 6 | 1.238<FWHM_IMAGE_H_E<2.052 | 12 262 | 3.87 | 7018 | 2.50 |
| 7 | −0.005<SPREAD_MODEL_Y_E<0.017 | 11 550 | 3.62 | 6603 | 2.30 |
| 8 | 0.461<FWHM_IMAGE_Y_E<2.099 | 10 768 | 3.34 | 6208 | 2.03 |
| 9 | Drop 99 in any I_E mag | 9450 | 2.89 | 4663 | 1.43 |
| 10 | −0.002<SPREAD_MODEL_I_E<0.004 | 6819 | 2.09 | 3445 | 1.05 |
| 11 | 1.127<FWHM_IMAGE_I_E<2.843 | 6614 | 2.03 | 3293 | 1.01 |

**Table A.5.** *Euclid* photometry of previously known non-benchmark objects in the $\sigma$ Orionis cluster sequence.

| RA (J2000) | Dec (J2000) | $I_E$ | $\sigma(I_E)$ | $Y_E$ | $\sigma(Y_E)$ | $J_E$ | $\sigma(J_E)$ | $H_E$ | $\sigma(H_E)$ |
|---|---|---|---|---|---|---|---|---|---|
| 84°.847 645 | −2°.682 660 | 20.445 | 0.002 | 17.812 | 0.002 | 17.583 | 0.001 | 17.508 | 0.001 |
| 84°.872 332 | −2°.777 320 | 21.207 | 0.003 | 18.451 | 0.003 | 18.196 | 0.002 | 18.043 | 0.002 |
| 84°.885 072 | −2°.872 183 | 24.299 | 0.027 | 20.923 | 0.016 | 20.547 | 0.009 | 20.055 | 0.006 |
| 84°.943 614 | −2°.406 478 | 21.158 | 0.003 | 18.269 | 0.003 | 18.127 | 0.002 | 17.920 | 0.002 |
| 84°.989 081 | −2°.835 013 | 23.618 | 0.016 | 20.300 | 0.011 | 20.028 | 0.007 | 19.749 | 0.006 |
| 85°.028 991 | −2°.601 451 | 22.725 | 0.008 | 19.478 | 0.005 | 19.124 | 0.003 | 18.861 | 0.003 |
| 85°.032 282 | −2°.376 239 | 23.945 | 0.022 | 20.758 | 0.017 | 20.284 | 0.009 | 19.915 | 0.007 |
| 85°.076 609 | −2°.385 794 | 20.358 | 0.002 | 17.994 | 0.003 | 17.216 | 0.001 | 16.513 | 0.001 |
| 85°.048 215 | −2°.859 726 | 24.400 | 0.039 | 21.159 | 0.017 | 20.872 | 0.011 | 20.705 | 0.010 |
| 84°.919 110 | −2°.653 550 | 18.348 | 0.001 | 16.570 | 0.001 | 16.416 | 0.001 | 16.196 | 0.001 |
| 84°.893 058 | −2°.646 380 | 18.266 | 0.001 | 15.986 | 0.001 | 15.967 | 0.001 | 15.882 | 0.001 |
| 84°.815 680 | −2°.640 655 | 18.387 | 0.001 | 16.209 | 0.002 | 16.075 | 0.001 | 16.024 | 0.001 |
| 84°.861 922 | −2°.615 620 | 18.952 | 0.001 | 16.585 | 0.001 | 16.452 | 0.001 | 16.414 | 0.001 |
| 85°.018 897 | −2°.611 691 | 18.877 | 0.001 | 16.491 | 0.001 | 16.351 | 0.001 | 16.613 | 0.001 |
| 85°.074 216 | −2°.448 392 | 19.842 | 0.002 | 17.473 | 0.002 | 17.312 | 0.001 | 17.164 | 0.001 |
| 85°.142 016 | −2°.434 096 | 20.055 | 0.002 | 17.779 | 0.002 | 17.424 | 0.001 | 17.179 | 0.001 |
| 84°.813 607 | −2°.364 092 | 19.135 | 0.001 | 16.728 | 0.002 | 16.615 | 0.002 | 16.525 | 0.002 |
| 84°.808 099 | −2°.272 735 | 21.907 | 0.005 | 18.837 | 0.007 | 18.606 | 0.005 | 18.353 | 0.004 |

**Table A.6.** *Euclid* objects of interest in the $\sigma$ Orionis region.

| Code | RA (J2000) | Dec (J2000) | $I_E$ | $\sigma(I_E)$ | $Y_E$ | $\sigma(Y_E)$ | $J_E$ | $\sigma(J_E)$ | $H_E$ | $\sigma(H_E)$ |
|---|---|---|---|---|---|---|---|---|---|---|
| A | 85.°162 830 | −2.°292 707 | 19.084 | 0.001 | 17.184 | 0.002 | 16.898 | 0.001 | 16.699 | 0.001 |
| B | 84.°807 391 | −2.°529 354 | 21.692 | 0.007 | 18.724 | 0.006 | 18.523 | 0.004 | 18.361 | 0.004 |
| C | 85.°036 499 | −2.°714 769 | 23.362 | 0.019 | 20.536 | 0.014 | 20.091 | 0.007 | 19.901 | 0.007 |
| D | 85.°119 119 | −2.°851 646 | 23.779 | 0.025 | 20.545 | 0.011 | 20.211 | 0.007 | 19.840 | 0.005 |
| E | 84.°892 801 | −2.°981 698 | 25.081 | 0.110 | 21.951 | 0.067 | 21.499 | 0.037 | 21.264 | 0.030 |
| F | 85.°146 780 | −2.°918 538 | 26.444 | 0.194 | 22.897 | 0.095 | 22.670 | 0.061 | 22.286 | 0.042 |
| G | 84.°818 225 | −2.°395 095 | 26.536 | 0.221 | 23.098 | 0.134 | 22.469 | 0.062 | 22.243 | 0.051 |

## Appendix B: Additional figures

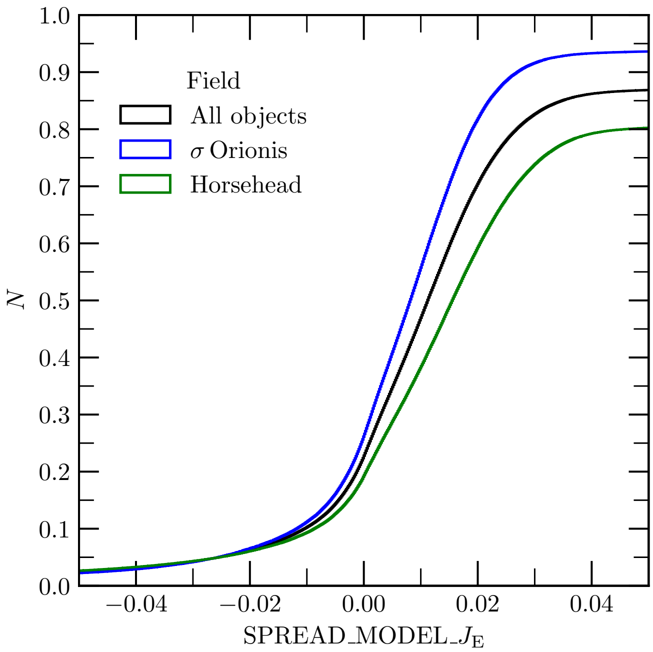


**Fig. B.1.** Cumulative distribution of spread model values for the *Euclid* $J_E$ band. The distribution of values in the low-reddening part corresponding to the $\sigma$ Orionis cluster is sharper than in the high-reddening part.

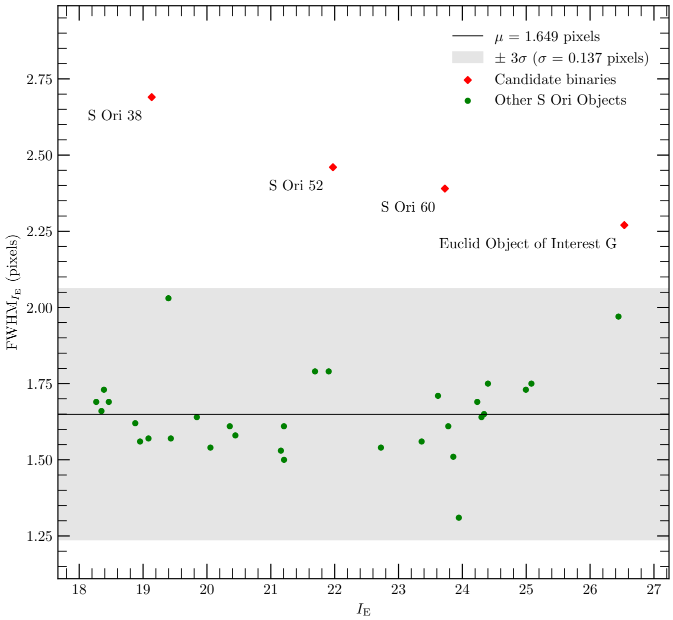


**Fig. B.2.** *Euclid* VIS FWHM (in pixels) versus $I_E$ apparent magnitude for objects confirmed by *Euclid* to be in the $\sigma$ Orionis cluster sequence. Both the FWHM and $I_E$ photometry values come from the ERO catalogue. Four objects were found to have FWHM values larger than the mean value of cluster members (more than $3\,\sigma$ significance) and hence are considered as possible binaries that deserve further scrutiny. Two of them are benchmark objects, namely (S Ori 52 and S Ori 60), one is a known object (S Ori 38), and the faintest one is a new discovery (*Euclid* object of interest G).

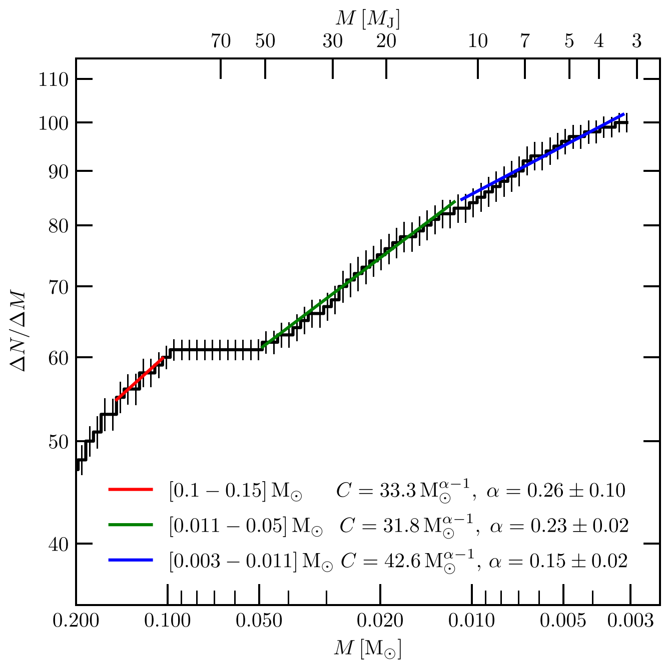


**Fig. B.3.** Unresolved binary-corrected very low mass *Euclid-Gaia* IMF of the $\sigma$ Orionis cluster with linear fits in three different mass regions. A 20% unresolved binary frequency of equal mass binaries has been assumed in the simulations.